Electronic and mechanical anharmonicities in the vibrational spectra of the H-bonded, cryogenically cooled X-HOCl (X=Cl, Br, I) complexes: Characterization of the strong anionic H-bond to an acidic OH group

Santino J. Stropoli,^a Thien Khuu,^a Mark A. Boyer,^c Natalia V. Karimova,^b Coire F. Gavin-Hanner,^c Sayoni Mitra,^a Anton L. Lachowicz,^a Nan Yang,^a R. Benny Gerber,*^{b,d}, Anne B. McCoy,*^c and Mark A. Johnson*^a

- 7 ^a Sterling Chemistry Laboratory, Department of Chemistry, Yale University, New Haven, CT 06520,
- 8 United States
- 9 bepartment of Chemistry, University of California Irvine, Irvine, California 92697, United
- 10 States

1

2

3

- ^c Department of Chemistry, University of Washington, Seattle, WA 98195, USA
- ^d Institute of Chemistry and The Fritz Haber Research Center, The Hebrew University, Jerusalem 91904,
- 13 Israel

18

19

20

21

2223

24 25

26

27

28

29

30

31

32

33

34 35

- ***Corresponding Authors:**
- 15 R. Benny Gerber: bgerber@uci.edu
- 16 Anne B. McCoy: abmccoy@uw.edu
- 17 Mark A. Johnson: <u>mark.johnson@yale.edu</u>

ABSTRACT

We report vibrational spectra of the H_2 -tagged, cryogenically cooled X^- ·HOCl (X = Cl, Br and I) ion-molecule complexes and analyze the resulting band patterns with electronic structure calculations and an anharmonic theoretical treatment of nuclear motions on extended potential energy surfaces. The complexes are formed by "ligand exchange" reactions of X⁻·(H₂O)_n clusters with HOCl molecules at low pressure (~10⁻² mbar) in a radio-frequency ion guide. The spectra generally feature many bands in addition to the fundamentals expected at the double harmonic level. These "extra bands" appear in patterns that are similar to those displayed by the X-HOD analogues, where they are assigned to excitations of nominally IR forbidden overtones and combination bands. The interactions driving these features include mechanical and electronic anharmonicities. Particularly intense bands are observed for the $v = 0 \rightarrow 2$ transitions of the out-of-plane bending soft modes of the HOCl molecule relative to the ions. These involve displacements that act to break the strong H-bond to the ion, which give rise to large quadratic dependences of the electric dipoles (electronic anharmonicities) that drive the transition moments for the overtone bands. On the other hand, overtone bands arising from the intramolecular OH bending modes of HOCl are traced to mechanical anharmonic coupling with the v = 1 level of the OH stretch (Fermi resonances). These interactions are similar in strength to those reported earlier for the X-HOD complexes.

I. INTRODUCTION

The molecular-level mechanics of the "anionic H-bond" to the OH group have been extensively explored in the binary complexes between water, methanol, and formic acid with the halide ions. A major conclusion from these efforts is that the observed spectra above 1000 cm⁻¹ are typically more complex than the simple three-band pattern [e.g., two OH stretches and the HOH intramolecular bend for X⁻·H₂O] predicted to occur at the harmonic level. Specifically, "extra bands" appear scattered across the spectrum that are traced to surprisingly strong mechanical (potential) and electronic (electric dipole) anharmonicities. These effects are well documented in the analysis of neutral van der Waals complexes, but are amplified in the case of the more strongly bound ionic systems. In the latter

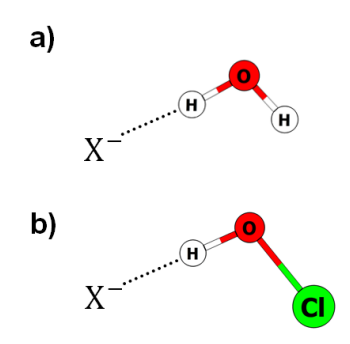


Figure 1. Comparison of the hydrogen bonding motifs in (a) X^- ·HOH and (b) X^- ·HOCl, where X = Cl, Br, or I.

case, the extra bands are due to the excitation of soft mode vibrational levels whose displacements break the directional hydrogen bonds. As such, linear vibrational spectroscopy provides a window into the topologies of the potential and dipole surfaces away from the equilibrium geometry. In this paper, we expand this survey to include the hydrogen bonds between halide ions and the more acidic HOCl molecule (pK_a values of 7.549 and 1410 for HOCl and H₂O, respectively), a choice that is motivated, in part, because of HOCl's importance in interfacial atmospheric chemistry. Both the H₂O and HOCl complexes with halides are observed to adopt the asymmetric, "single ionic H-bonded" geometries indicated in **Figure 1**, in which an OH group is bound to the ion, while either the Cl or H atoms are non-bonded. The band assignments are aided by comparison with the behaviors of the X^- HOD isotopomers with the OH group bound to the ion, and taking into account the stronger H-bonds between the halide ions and HOCl.

II. METHODS

IIA. Experimental details

The $X^-\text{HOCl}$ (X = Cl, Br, and I) complexes were formed in the gas phase using the so-called "ligand switching" approach that involves displacement of one (or more) water molecule(s) in the reaction:

$$X^{-} \cdot (H_2 O)_n + HOCl \rightarrow X^{-} \cdot HOCl + nH_2 O$$
 (1)

The $X^-(H_2O)_n$ clusters were formed in an electrospray ionization source and injected into a series of radiofrequency (RF) ion guides as described in detail in **Section S1** of the **Supplementary Material**. Reaction (1) was carried out in a quadrupole guide filled with HOCl gas (preparation described in **Section S2**) at a pressure of $\sim 10^{-2}$ mbar. The product ions were then transferred to a three-dimensional quadrupole trap (R.M. Jordan) cooled by a closed-cycle He cryostat to about ~ 20 K, where H₂ molecules were condensed onto the X^- HOCl binary complexes by pulsing a buffer gas mixture containing $\sim 20\%$ H₂ in a balance of He. Mass spectra displaying the products of collisions between HOCl and X^- ·(H₂O)_n are presented in **Figure S1**. The dominant species that are generated correspond to the uptake of HOCl onto the parent X^- ·(H₂O)_n clusters to yield X^- ·(HOCl)·(H₂O)_n. While the presence of multiple chlorine and

bromine isotopes results in a number of mass degeneracies between the products and the parent cluster series, the X⁻(HOCl)·(H₂O)_n species containing the most naturally abundant ³⁵Cl and ⁷⁹Br isotopes (i.e., the major products) are unique and thus easily distinguished. The vibrational spectra were recorded over

79 the range $1000 - 4000 \text{ cm}^{-1}$ by IR photodissociation of weakly bound H₂ molecules:

$$X^{-} \cdot HOCl \cdot H_2 + h\nu \rightarrow X^{-} \cdot HOCl + H_2$$
 (2)

in a linear action regime in a triple-focusing photofragmentation mass spectrometer. ¹⁸⁻²⁰ The resulting band patterns are analyzed using an anharmonic treatment of the nuclear motions on extended surfaces of the potential energy and electric dipole moments.

IIB. Theoretical details

Second-order vibrational perturbation theory calculations were performed using the PyVibPTn package, ^{21, 22} which is based on the formulation of perturbation theory described by Sakurai. ²³ These calculations utilized the quartic expansions of the potential energy surface evaluated within the Gaussian 16²⁴ software package. Our implementation of VPT2 allows us to evaluate transitions to states with more than two quanta of excitation, and provides greater flexibility in the choice of the resonances considered than does the standard implementations of VPT2 in Gaussian. These calculations were augmented by one-dimensional calculations of the vibrational levels of the OH stretch and out-of-plane bend based on cuts through the full-dimensional surface, with all of the coordinates except the OH bond length constrained to their equilibrium values, and the three O-H···X⁻ atoms constrained to be collinear. Additional details about the VPT2 and the one-dimensional calculations are provided in **Section S3** of the **Supplementary Material**. Natural bond orbital²⁵ calculations were performed to obtain the partial charges of the atoms as the hydrogen atom is displaced either along the OH bond or perpendicular to the plane containing the other three atoms. All electronic structure calculations were performed at the MP2/aug-cc-pVTZ level of theory/basis using Gaussian 16. The corresponding aug-cc-pVTZ-pp basis set and effective core potential were used as given in refs. 26 and 27 for Γ . ^{26, 27}

III. RESULTS AND DISCUSSION

IIIA. Comparison between the vibrational spectra of X-HOD and X-HOCl in the regions of the OH stretch and bend fundamental transitions

The H₂-tagged vibrational predissociation spectra of the three $X^-\text{HOCl}$ ions are compared with those reported earlier¹ for the $X^-\text{HOD}$ series in **Figure 2**. The band highest in energy in the $X^-\text{HOCl}$ series is due to the activation of the nominally forbidden H₂ stretch (v_{H_2}) when bound to an ion.²⁸ The calculated structures of the H₂ ternary complexes are shown in **Figure S2**, where the H₂ molecule is found to preferentially bind onto the halide, as described in **Section S4**. Note that the asymmetrical $X^-\text{HOD}$ clusters occur in two isomeric forms (isotopomers) according to whether the H or D atom is bound to the halide. Bands assigned to the D-bound isotopomer are colored gray in **Figures 2d-f** to minimize the spectral clutter.

The bands due to the X $\dot{}$ -HOD isotopomer with the OH group bound to the ion that occur above 2500 cm $^{-1}$ are dominated by the strong bound OH stretch fundamentals (denoted $v_{\rm OH_b}$ and highlighted in red in **Figures 2d-f**), which are observed to evolve to higher energy from Cl to I. These generally occur

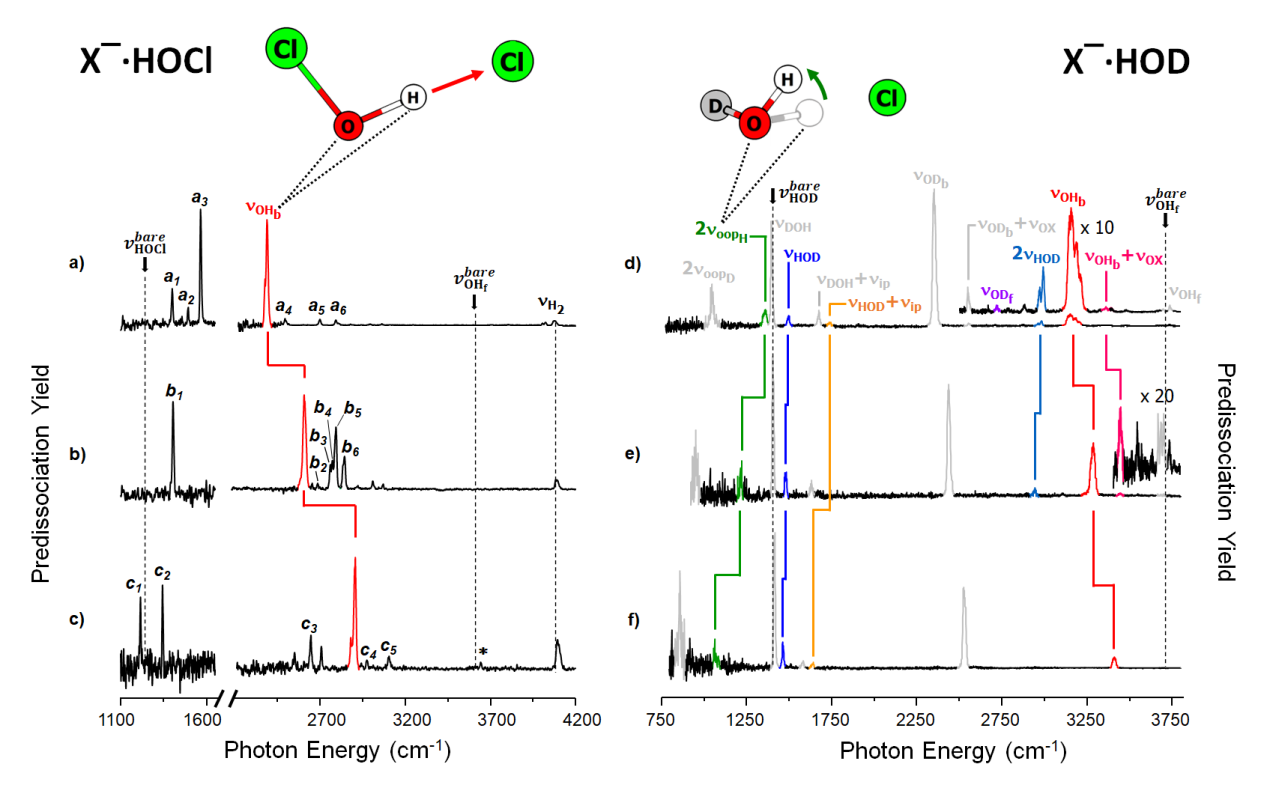


Figure 2. Comparison between the vibrational predissociation spectra of the H₂-tagged (a) Cl $^-$ HOCl, (b) Br $^-$ HOCl, and (c) $^-$ HOCl binary complexes and their Argon-tagged (d) Cl $^-$ HOD, (e) Br $^-$ HOD, and (f) $^-$ HOD counterparts. The bound OH stretching (v_{OH_b} , left) and the H out-of-plane overtone ($^-$ 2 v_{ooph} , right) bending motions are depicted inset. The bands presented in gray in (d)-(f) are due to the isotopomer with the OD group bound to the ion, X $^-$ DOH. Literature values of the OH bending and free OH stretching modes for neutral HOD³⁵ and neutral HOCl^{33,36} ($v_{HOD/Cl}^{bare}$ and $v_{OH_f}^{bare}$, respectively), are indicated by black arrows in (a) and (d). The band assignments for the X $^-$ HOD spectra are reproduced with permission from ref. 1 and are color-coded to highlight features primarily due to the OH stretch fundamental (red), the fundamentals and overtones of the HOD bend (blue), and the oop frustrated rotation (green). Bands labels are assigned in **Tables I-II**. The * feature in (c) indicates the possible formation of a weakly abundant isomer with a free OH group.

along with weaker multiplet structures that arise from anharmonic interactions, as discussed in detail in refs. 1-2 (band labels are elaborated in **Tables I-II**). As is the case with X $^-$ HOD, there are several stable isomers of X $^-$ HOCl: the hydrogen bonded form displayed in **Figure 1b**, the halogen-bound X $^-$ ClOH, ²⁹⁻³² and possibly the binary complex in which XCl is bound to OH $^-$. The spectra of the latter isomers are expected to contain a peak associated with a free or weakly perturbed OH stretch in the range of 3500-3700 cm $^{-1}$. The lack of such features when X = Cl and Br and the very weak feature near 3650 cm $^{-1}$ when X = I (denoted by * in **Figure 2c**) leads us to conclude that the carrier of the spectra shown in **Figures 2a-c** are indeed the hydrogen bonded X $^-$ HOCl structures. Like the spectra of the X $^-$ HOD clusters, those of the X $^-$ HOCl series (**Figures 2a-c**) above 2500 cm $^-$ 1 are similarly dominated by a strong band with halidedependent shifts that are assigned to the v_{OH_b} fundamentals of the bound OH group (again highlighted in red). Note that the shifts of these bands (relative to the free OH band of bare HOCl³³, black arrow labeled $v_{OH_f}^{bare}$ in **Figure 2a**) are much larger ($^-$ 3×) than the shifts in the v_{OH_b} bands of X $^-$ HOD, while the linewidths (with the exception of that in Cl $^-$ HOD) are comparable. As such, these complexes do not

display the typical behavior of strong H-bonds where the linewidths increase along with the relative intensity.³⁴

In the lower energy region near the HOD bend fundamental (1400 cm⁻¹ in bare HOD), the X-HOD spectra (Figures 2d-f) do not exhibit a dominant band, but rather appear with two features of comparable intensity. These have been assigned to the bend fundamental (v_{HOD} , blue) and the $v = 0 \rightarrow 2$ overtone of the frustrated out-of-plane rotation $(2v_{\text{oop_H}}, \text{green})$ of the water molecule. Weaker combination bands are also present that arise from excitation of the bend fundamental with one quantum in the in-plane frustrated rotation ($v_{HOD} + v_{ip}$, orange). Note that the bend fundamental displays a gradual red-shift down the halide series (~20 cm⁻¹ per halogen from Cl⁻ to I⁻), and appears farthest above the bend in the bare HOD molecule³⁵ (black arrow in **Figure 2d** denoted $v_{\rm HOD}^{bare}$) in the Cl species (by 105 ${\rm cm}^{-1}$). The incremental shifts in the $2v_{{
m oop}_H}$ feature, on the other hand, are much larger with changes of 142 and 159 cm⁻¹ from Cl⁻ to Br⁻ to I⁻. The lower energy range of the X⁻·HOCl spectra also displays multiplet structures (for Cl and I) near the bend fundamental of bare HOCl36 (black arrow in Figure 2a denoted v_{HOCI}^{bare}) which are strongly dependent on the halide such that bands red-shift down the series. In this case, however, it is not obvious by inspection which of these are primarily due to the bend fundamentals of the X⁻·HOCl complexes. We postpone discussion of the mechanics underlying these qualitative trends in the OH bending region to Section IIIC after first considering the electronic character of the strong ionic H-bond.

IIIB. Quantifying frustrated intracluster proton transfer and associated charge delocalization in the strong anionic H-bond

Very large $v_{\rm OH_b}$ red shifts have been reported in the B $^-$ ·H₂O complexes (B = O, OH, and F) and analyzed in the context of the increasing electric field around the smaller ions, which is in turn correlated with the stronger basicities of the lighter halides.⁴ The extreme case of OH $^-$ ·H₂O, for example, occurs as a quasi-symmetrical [HO···H···OH] $^-$ structure with an equally shared proton,^{37, 38} thus corresponding to a three-center, two electron covalently bound system akin to the classic case of FHF $^-$.³⁹ From the perspective of acid-base interactions, the bound OH stretching fundamental energies reflect the energetics of the so-called "frustrated intra-cluster proton transfer" (FPT) reactions.^{4, 40} These are the cluster analogues of the familiar base hydrolysis reactions in aqueous electrolyte chemistry:

$$X^- + H_2O \to HX + OH^-$$
 (3)

The mechanics associated with FPT qualitatively account for both the large intensity and extreme red-shift of the bound OH stretching fundamental relative to the behavior of a generic free OH group with frequency $v_{\rm OH_f} \sim 3700~{\rm cm}^{-1}.^{41}$ This is illustrated by the shapes of the potential energy curves calculated for the parallel displacement of the shared proton from the oxygen (O) atom to the Cl⁻ ion displayed in the lower panel of **Figure 3** (red and black curves for Cl⁻·HOCl and Cl⁻·HOD, respectively). In particular, the attractive outer region on the potential curve calculated for the HOCl system displays an inflection point near 1.35 Å. This occurs when the system adopts electron configurations associated with the ClH···OCl⁻ partial proton transfer, thus driving down the v=1 energy level in the more acidic OH group of HOCl (proton affinities of OH⁻ and OCl⁻ of 1633^{42} and 1502^{43} kJ/mol, respectively). As is seen by the energy levels calculated based on these one-dimensional cuts, in the case of Cl⁻·HOCl, the level with one

quantum in the OH stretch samples this region of the potential, while for Cl⁻·HOD, the wave function remains localized in the part of the potential that corresponds to the Cl⁻·HOD complex.

To illustrate the changes in the electronic wavefunctions along the FPT coordinate, the upper panel of Figure 3a compares the natural charges⁴⁴⁻⁵¹ on the Cl⁻ anionic center for Cl-HOD (black) and Cl⁻·HOCl (red). The magnitude of the effective charge on the Cl⁻ ion decreases as the shared proton approaches it (i.e., as r_{OH} increases), forming a partially covalent interaction in the early stage of the FPT reaction. The intrinsically more responsive HOCl system with respect to charge redistribution, combined with the larger amplitude of the OH displacement in the v = 1 level, account for the increased IR transition moment for the OH stretching fundamental in the X-HOCl systems. Both the degree of charge displacement and the lowering of the potential are directly reflected in the intensity (see calculated values in Table II) and red-shift of the v_{OHb} fundamental in the Cl⁻·HOCl spectrum.

IIIC. Disentangling assignments of the HOD bending fundamentals and soft mode overtones

The directional nature of the strong H-bonds

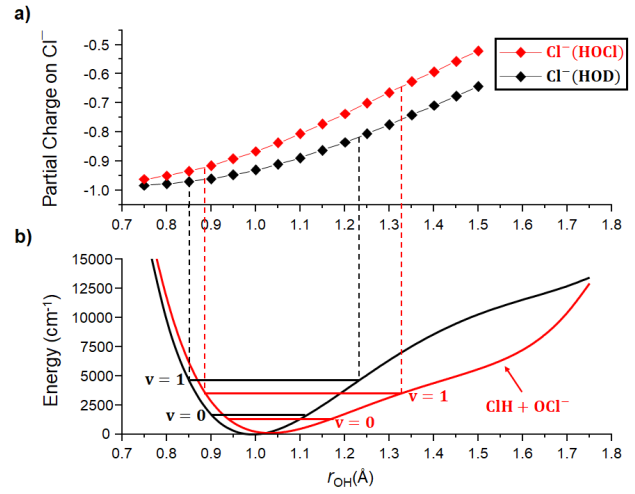


Figure 3. (a) Partial charges on the nominal Cl $^-$ moiety derived from an NBO analysis of electronic wave functions obtained at the MP2/aug-cc-pVTZ level of theory/basis and (b) one-dimensional potential surfaces as a function of the displacement of the shared H atom (r_{OH}) with the Cl $^-$ ···O distance fixed at the equilibrium length for Cl $^-$ ·HOCl (red) and Cl $^-$ ·HOD (black). The energies of the v=0 and 1 levels of each OH stretching mode are indicated with solid lines, and the classical turning points associated with the v=1 levels are indicated by color-coded dashed vertical lines. The distortion in the Cl $^-$ ·HOCl potential near 1.6 Å reflects the "shelf" arising from intra-cluster frustrated proton transfer (FPT).

in both HOD and HOCl systems has important consequences on spectral behavior in the 1000-1500 cm⁻¹ region of OH bending fundamentals. The role of anharmonicities is immediately clear, for example, by the fact that only a single fundamental in the HOCl bend is expected in this region, and is in all cases calculated to fall quite close to that of the isolated HOCl molecule as indicated in **Tables I-II**. Although a feature is indeed observed near $v_{\text{HOCl}}^{\textit{bare}}$ for all three ions, this band (labeled a_1 in **Figure 2a** and c_2 in **Figure 2c**) is much weaker than the very strong band (labeled a_3 in **Figure 2a**) higher in energy at 1564 cm⁻¹ in Cl⁻HOCl and similar in strength to a band lower in energy at 1206 cm⁻¹ (labeled c_1 in **Figure 2c**) in Γ -HOCl. For both X = Cl and I, this extra band lies very close to the calculated $v = 0 \rightarrow 2$ overtone transition associated with the out-of-plane (oop) frustrated rotation of the HOCl moiety relative to the X-O axis (denoted $2v_{\text{oop}_H}$) with displacements illustrated schematically at the top right of **Figure 2**. The observation that one of the features lies close to the harmonic value for $2v_{\text{oop}_H}$, and that it retains its large intensity as its frequency is tuned through the vicinity of the bend fundamental ($v_{\text{HOCl}}^{\textit{bare}}$), rule out intensity borrowing through mechanical anharmonicity as the primary cause for the unusually strong oscillator strength for this feature. The $2v_{\text{oop}_H}$ overtone transitions were also found in the X⁻·HOD spectra (green in the right panel of **Figure 2**) with intensities that were traced to the modulation of the large intra-

complex charge-transfer contribution in the equilibrium configuration upon displacement along the oop coordinate. This motion rotates the OH group off-axis, effectively breaking the strongly directional H-bond and therefore inducing relaxation of the charge back onto the X^- atom. This effect has been analyzed at length, and the large associated changes in the dipole moments along the X-O axes give rise to surprisingly strong $v = 0 \rightarrow 2$ overtone transitions in the $v_{\text{oop}_{H}}$ and in-plane rotation (v_{ip}) modes. This is a manifestation of electronic anharmonicity, where the quadratic dependence of the dipole moment on nuclear displacements drives the transition moments for IR excitation. The strongly directional hydrogen bond is also responsible for the shift of v_{HOCl} to higher frequencies as the interaction with the smaller halide ion increases. Explicit details of the relative contributions to the fundamentals and overtones are presented in **Section S5** of the **Supplementary Material**.

Table I. Assignments of experimentally observed frequencies (cm⁻¹) for the X^- HOCl complexes, accurate to within ± 4 cm⁻¹. Labels correspond to those indicated in **Figures 2 (a)-(c)**.

Label	Assignment	Cl-·HOCl	Br [−] ·HOCl	I-HOCl
a_1, c_2	OH Bend	1396		1341
a_2	OH Bend + In-Plane HOCl Rotation	1493		
a_3, b_1, c_1	H Out-of-Plane Overtone	1564	1399	1206
$v_{ m OH_b}$	Bound OH Stretch	2385	2603	2903
a_4, b_2, c_4	Bound OH Stretch + In-Plane HOCl Rotation	2490	2685	2974
a_5, b_6, c_5	Bound OH Stretch + Ion-HOCl Stretch	2696	2841	3100
$a_6, b_3/b_4/b_5, c_3$	OH Bend Overtone	2788	2782^{a}	2642
$v_{ m H_2}$	H ₂ Stretch	4079	4090	4106

^a value taken as the centroid of the triplet observed at 2758, 2768, and 2790 cm⁻¹.

Table II. Calculated vibrational frequencies (cm⁻¹) for the X⁻·HOCl complexes determined at the MP2/aug-cc-pVTZ level of theory/basis with VPT2 anharmonic correction. Calculated spectra were empirically shifted to recover the experimentally observed positions of the bound OH stretch and out-of-plane bend overtone transitions as described in **Section S3** of the **Supplementary Material**. Unshifted values are reported in **Figures S6** and **S7**. Intensities (km/mol) are listed in in paratheses next to each value. Values with *E* and *M* subscripts denote transitions that are allowed by primarily electronic or mechanical anharmonicity, respectively, determined by the ratio of the electronic contribution to the transition moment to the mechanical contribution based on analysis of the deperturbed levels, as described in **Section S3** of the **Supplementary Material**. Transitions with *E:M* ratios greater than 3/2 are assigned *E*, while those less than 2/3 are assigned *M*. The *E/M* label indicates that the transition moment arises from both electronic and mechanical contributions in roughly equal proportion. The intensities of transitions to states with one quantum of excitation are well-captured by a linear dipole/harmonic oscillator approximation and are not labeled. Cases where mixing of the deperturbed states leads to a change in the intensity of more than a factor of two are labeled with *F* subscripts.

Label	Assignment	Cl⁻·HOCl	Br ⁻ ·HOCl	I-HOCl
$v_{ m HOCl}$	OH Bend	1398 (48)	$1368 (4)_F$	1346 (36)
$v_{ m HOCl} + v_{ m ip}$	OH Bend + In-Plane HOCl Rotation	$1497 (5.7)_E$	$1454 (3.6)_E$	$1418 (1.3)_E$
$2v_{\mathrm{oop_H}}$	H Out-of-Plane Overtone	1563 (141) $_{E/M}$	$1398 (121)_E$	$1207 (50)_E$
$v_{ m OH_b}$	Bound OH stretch	2384 (2577)	2602 (1863)	2903 (1912)
$v_{\mathrm{OH_b}} + v_{\mathrm{ip}}$	Bound OH Stretch + In-Plane HOCl Rotation	$2495 (114)_M$	$2675 (6.3)_M$	$2978 (181)_M$
$v_{\mathrm{OH_b}} + v_{\mathrm{OX}}$	Bound OH Stretch + Ion-HOCl Stretch	$2697 (93)_M$	$2842 (180)_F$	$3116 (4.7)_M$
$2v_{ m HOCl}$	OH Bend Overtone	$2816 (177)_F$	$2809 (549)_F$	$2609 (247)_F$

To investigate the magnitudes of the electronic anharmonicities expected for the X-HOCl systems, we calculated the vector contributions to the dipole moment as a function of displacements along the out-ofplane coordinate (Q_{oop}) , with the results presented in **Figure 4**. In the Cartesian axes defined in the inset of Figure 4a, the dipole moment perpendicular to the bond, $\mu_{\perp a}$, in the direction out of the plane defined by the equilibrium structure, is observed to depend linearly on Q_{oop} (**Figure 4a**). On the other hand, the component parallel to the O···Cl⁻ axis, $\mu_{\parallel_{\mathbf{r}}}$, displays a quadratic dependence on Q_{oop} (**Figure 4b**). The third component, $\mu_{\parallel_{V}}$ (y-axis), which is also in the heavy atom plane, is nearly zero for Cl⁻·HOD and is an order of magnitude smaller than the xcomponent in Cl-HOCl as shown in Figure S5. Note that the magnitude of the change in μ_{\parallel_x} is much larger for the HOCl complexes than for HOD, which is again consistent with the larger degree of charge transfer at the equilibrium geometry, while the change in μ_{\perp_z} is only slightly larger for the HOD complex. The strong halide dependence of the $v_{\text{oop}_{H}}$ frequency is evident in the $2v_{\text{oop}_{H}}$ bands in the X-HOD complexes (green in Figures 4c, 4e, and 4g), while the bend fundamental (v_{HOD} , blue) is only weakly dependent on the halide. The response of the $v_{\text{oop}_{H}}$ mode thus directly reflects the stronger H-bonds in the lighter halides that act to stiffen the force constants for the outof-plane vibrations. With the X-HOD behavior in mind, it is straightforward to assign the strongly halide-dependent bands in the X⁻·HOCl complexes (green in **Figures** 4d, 4f, and 4h) to the $2v_{\text{oop}_H}$ transitions, while those that appear close to the neutral HOCl bend are due to the bend fundamentals of the HOCl moieties (v_{HOCl} , blue).

217

218

219

220

221

222

223

224

225

226

227

228

229

230

231

232

233

234

235

236

237238

239

240

241

242

243

244

245

246247

248

249

250

251

252

253

254

255

256

257

258

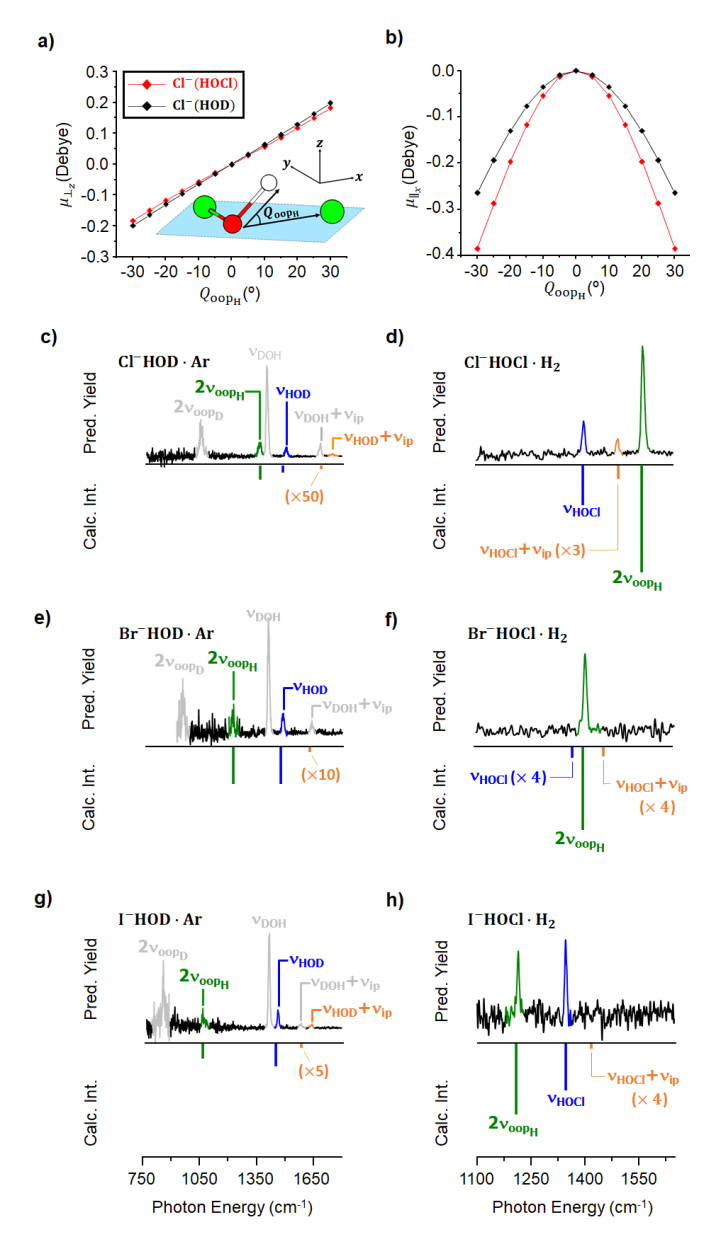


Figure 4. Dependence of the μ_{\perp_z} (a) and μ_{\parallel_x} (b) vector components of the electric dipole moment as a function of displacements along the out-of-plane frustrated rotation, Q_{oop} , for Cl⁻·HOCl (red) and Cl⁻·HOD (black). The Q_{oop} coordinate and x, y, and z axes are defined by the inset in (a). The expanded OH bending region of the experimental X⁻·HOD (left) and X⁻·HOCl (right) spectra are reproduced from Figure 2 in (c)-(h), along with corresponding inverted stick spectra calculated at the MP2/aug-cc-pVTZ level of theory/basis with VPT2 anharmonic correction. Calculated spectra were empirically shifted to recover the experimentally observed positions of the $2v_{\rm ooph}$ transition as described in section S3 of the Supplementary Material. Calculated spectra without this shift are included in Figure S6.

Closer inspection of the calculated anharmonic behavior of the X-HOCl complexes in the bending region indicates that the v = 2 levels of the $2v_{\text{oop}_H}$ mode and the v = 1 level of the HOCl bend, which both have A' symmetry, are coupled through a Fermi interaction. The approximate magnitude of this effect is encoded in the $\frac{1}{2}F_{oob}Q_{oop}^2 \times Q_{bend}$ cubic term in the Taylor expansion of the potential energy. Incorporation of this term in a degenerate perturbation theory calculation yields coupling matrix elements of 9, 13 and 17 cm⁻¹, respectively (see **Table III**) for Cl, Br and I. In contrast to the prototypical situation where the overtone transition has a small cross section, both the unperturbed v_{HOCl} and $2v_{oop_H}$ transitions are calculated to occur with significant intensities. In the Cl⁻·HOCl case, the oop overtone transition carries about three times the intensity of that calculated for the bend fundamental (see Table II). This results in an interference term that alters the distribution of oscillator strength among the two bands that result from excitation of the perturbed excited state levels. To gauge how this effect impacts the observed spectra, the calculated zero-order $2v_{\text{oop}_H}$ level was shifted to recover the observed position of this band in the spectra for each of the X-HOCl complexes, and the Fermi analysis was repeated using the calculated zero-order v_{HOCI} and Fermi coupling constant. This procedure recovers the intensities of the two bands in the Cl⁻·HOCl and Γ·HOCl complexes (green and blue inverted bars in **Figures 4d** and 4h; the spectra obtained without this shift are provided in Figure S6). Interestingly, this procedure predicts that the transition moment to one of the two transitions is effectively cancelled by the interference term (inverted blue v_{HOCl} bar in Figure 4f), accounting for the fact that only one band is observed for the Br-HOCl complex in the bending region (as opposed to being a case of accidental degeneracy). As such, we report in **Table II** the expected frequency of the fundamental that is too weak to be observed here. Note that the deperturbed levels (i.e., calculated energies used in the 2×2 Fermi analysis) yield a smooth evolution of the zero-order bends (decreasing from Cl to I) similar to that observed for X-HOD, while the observed transitions in HOCl are nearly identical in the Cl and Br spectra and then red-shift in the I complex.

259

260

261

262

263

264

265

266

267

268269

270

271

272273

274

275

276

277

278

279

280

281 282

283

284

285

286287

288

289

290

291292

293

294 295 Close inspection of **Figure 4d** reveals that there is one additional feature in the Cl $^-$ HOCl spectrum in the bending region (orange) that is anticipated by the VPT2 calculation. This feature is traced to the combination band involving excitation of the bending fundamental along with one quantum of the in-plane frustrated rotation ($v_{\text{HOCl}} + v_{ip}$). This is again similar to the situation encountered in X $^-$ HOD clusters, and arises due to the strong dependence of the electric dipole surface on both the HOD bending and the in-plane displacement of the OH group. As such, this represents a case where the oscillator strength for a band forbidden in the double harmonic approximation is activated by electronic anharmonicity. Having assigned the $2v_{\text{oop}_{\text{H}}}$ transitions, we note that there is a pronounced anti-correlation between the frequencies of the $v_{\text{oop}_{\text{H}}}$ and $v_{\text{OH}_{\text{b}}}$ fundamentals. In particular, as the stronger interactions with the acid act to lower the bound OH stretching potentials due to the emergence of the FPT shelf (see **Figure 3b**), these stronger bonds are harder to break by modes whose displacements are perpendicular to the bond, and thus lead to blue-shifts in the oop fundamentals (as evidenced by the observed behavior of the overtones).

IIID. Multiplet structures near the bound OH stretching fundamentals

296

297

298

299

300

301

302 303

304

305

306

307

308

309

310

311

312

313

314

315

316

317

318 319

320

321

322

323

324

325

326

327

328

329

330

331

332

333

334

335

336

We next address the X-HOCl band patterns observed in the region of the strong $v_{\rm OH_h}$ fundamentals near 2700 cm⁻¹. The appearance of extra bands in this region have been analyzed in the X-H₂O, X-HOD, and X⁻·D₂O spectra, and are remarkably complex in the case of the I-H₂O system reported in 2020.⁵² The dominant effect here is the strong Fermi-type resonance interaction between the v_{OH_h} and the v = 2 level of the corresponding OH bend, which in water occurs with a characteristic matrix element of about 35 cm⁻¹.⁵³ In the X⁻·HOD series, this accounts for the enhancement of the OH bend overtones ($2v_{HOD}$, blue in Figures 2d and **2e**) near 3000 cm⁻¹. The increase in the $2v_{\text{HOD}}$ band intensity from X = Br to Cl occurs because the $v_{\rm OH_h}$ fundamental is lowered in the Cl-HOD complex, bringing its v = 1 level closer in energy to the v = 2level of the bend. In addition to the bend/stretch Fermi resonances, the OH stretching bands in X-HOD also occur with weaker combination bands associated with the ion-water stretching (v_{OX}) and in-plane frustrated rotation (v_{ip}) soft modes. Because the fundamentals of these modes are typically out of the range of table-top IR laser systems such as that used here, the combination bands are particularly useful because they provide benchmarks for intermolecular potentials that describe the ion-molecule interactions. In the X-H₂O series, for example, this procedure provided values for all six fundamentals.⁵⁴

Turning to the X⁻·HOCl series, the analysis in Section IIIB regarding the assignments of the intramolecular HOCl bending levels provides information

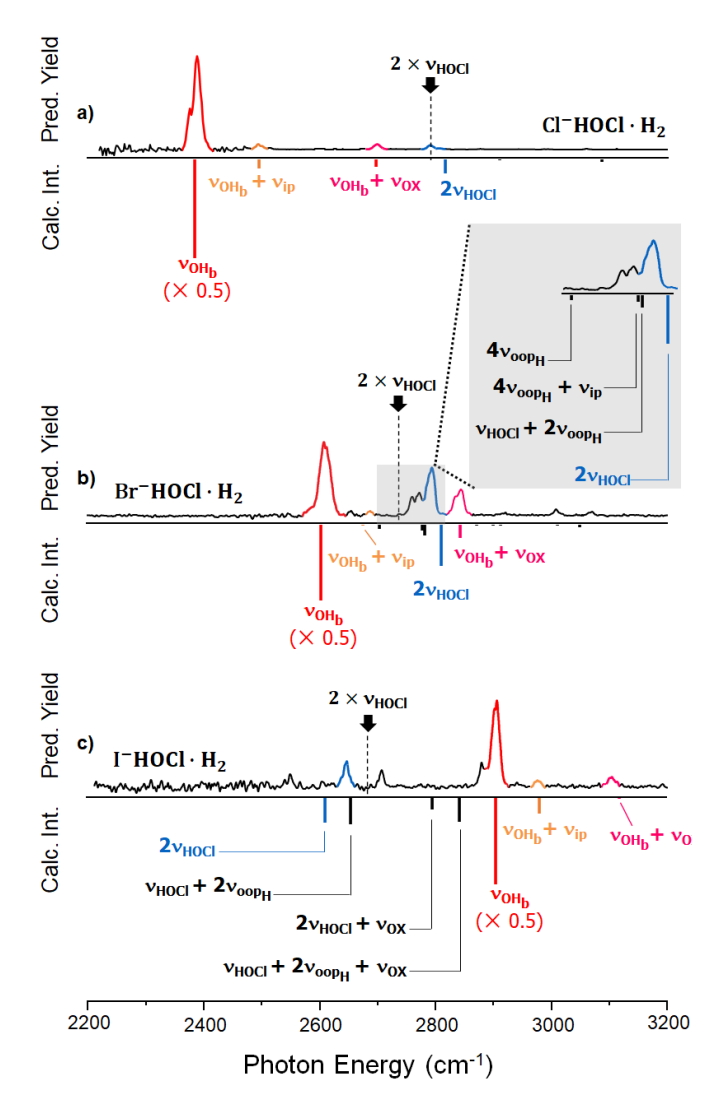


Figure 5. Expanded region of the bound OH stretching fundamentals for the H₂-tagged (a) Cl⁻·HOCl, (b) Br⁻·HOCl, and (c) I-HOCl binary complexes. The corresponding inverted stick spectra calculated at the MP2/aug-cc-pVTZ level of theory/basis with VPT2 anharmonic correction (see Section S3 of the Supplementary Material for details) are presented below each experimental spectrum in (a)-(c). Calculated spectra were empirically shifted to recover the experimentally observed positions of the $v_{\rm OH_b}$ transition. Calculated spectra without this shift are included in Figure S7. The approximate energies of the v = 2 OH bending level in the harmonic limit (calculated as $2 \times$ the experimental v_{HOCl} value for Cl⁻·HOCl and l⁻·HOCl, and 2 × the theoretical v_{HOCl} value from Figure 4 for Br-HOCl) are indicated by the black 2 x v_{HOCl} arrows. The multiplet structure of Br-HOCl (grey rectangle) is expanded as an inset in (b).

Table III. H_{Fermi} matrix elements coupling the v_{OH_b} v = 1 and v_{HOCl} v = 2 levels (shaded grey) and between the v_{HOCl} v = 1 and v_{oop_H} v = 2 levels (unshaded) of the X $^-$ HOCl complexes, generated from the cubic terms in the expansion of the potential energy. Experimental values were determined empirically by fits to a 2 × 2 Fermi Resonance model as previously described⁵⁵ (peak fits are provided in **Figure S8**), while calculated values were generated in the VPT2 method used in **Table II**. Citations for experimental values obtained in previous studies are included in the table entry.

Species	Experiment (cm ⁻¹)	Theory (cm ⁻¹)	Theory (cm ⁻¹)
	$v_{\mathrm{OH_b}} \times 2v_{\mathrm{HOCl}}$	$v_{\mathrm{OH_b}} \times 2v_{\mathrm{HOCl}}$	$v_{\mathrm{HOCl}} \times 2v_{\mathrm{oop_H}}$
Cl ⁻ ·H ₂ O	33 ⁵³	38	
Cl-·HOD	62 ⁵⁶	78	
Cl ⁻ ·HOCl	66	88	9
Br [−] ·H ₂ O	30	41	
$Br^{-}\cdot HOD$	87	82	
Br ⁻ ·HOCl	88	102	13
$I^-\cdot H_2O$	37	44	
I⁻·HOD		86	
□-HOC1	99	116	17

344

345

346

347 348

349

350

351 352

353

354

355

356 357

358

359

360 361

362

363

337

338

339

340 341

342

necessary to estimate the patterns of levels that occur near the $v_{\rm OH_h}$ fundamentals (red in Figure 2). We begin the spectral decomposition by approximating the energy of the v = 2 OH bending level in the harmonic limit (2 \times v_{HOCl}) using the experimentally measured position of v_{HOCl} for Cl and I^- HOCl and the calculated position of v_{HOCl} from Figure 4 (blue) for Br $^-$ HOCl. These values are included as black arrows in Figure 5, and it is clear that these levels effectively cross over the v = 1 levels of the bound OH stretch, becoming nearly degenerate in the Br complex. This behavior is, in fact, remarkably similar to that of Br $^-$ ·H₂O, ⁵⁶ where the nominal v_{OH_b} fundamental appears as a doublet with nearly equal intensity in each member, split apart by about 60 cm⁻¹. Because in this case the zero-order $2v_{HOH}$ carries very little oscillator strength, the splitting immediately reveals the H_{Fermi} coupling matrix element to be ~30 cm⁻¹ as discussed above. The Br-HOCl spectrum is more complex in that it displays a multiplet structure with a cluster of overlapping peaks near 2800 cm⁻¹. Because the zero-order levels are far apart in the Cl and Γ -HOCl complexes, a similar 2 \times 2 deperturbation scheme to recover the separation and relative intensities of the observed v_{OH_b} (red) and $2v_{HOCl}$ (blue) transitions yields effective H_{Fermi} values of 66 and 99 cm⁻¹, which are included in **Table III**. Like the case in the X⁻·HOD spectra, weaker peaks appear above the dominant v_{OH_b} features in the X $^-$ ·HOCl spectra. The displacements of these above the $v_{\rm OH_b}$ fundamentals and their relative intensities are accurately recovered by an anharmonic VPT2 analysis, as indicated by the inverted bars in Figures 5a and 5c. These are assigned to combination bands between v_{OH_b} v = 1 and one quanta of the in-plane rotation (v_{ip} , orange) and ion-HOCl stretching $(v_{OX}, pink)$ motions. The band positions are collected in **Table I** and provide useful estimates of the soft mode fundamentals presented in Table IV.

Table IV. Experimental (theoretical) vibrational frequencies of the fundamental IR transitions of X^- ·HOCl complexes. In cases where experimental values are unavailable, only the theoretical values are shown. Theoretical values were determined at the MP2/aug-cc-pVTZ level of theory/basis with VPT2 anharmonic correction and when the values of the calculated energies of the $v_{\rm OH_b}$ and $2v_{\rm oop_H}$ transitions were empirically shifted to recover the experimentally observed positions as described in **Section S3** of the **Supplementary Material**.

Label	Assignment	Cl⁻·HOCl	Br⁻∙HOCl	Г∙НОСІ
$v_{ m ip}$	In-Plane HOCl Rotation	$105^a (103)$	(83)	$71^{a}(71)$
$v_{ m OX}$	Ion-HOCl Stretch	311^a (282)	(235)	$197^a (199)$
$v_{ m O-Cl}$	O-Cl Stretch	(771)	(767)	(666)
$v_{ m oop_H}$	H Out-of-Plane Rotation	$782^b (782^c)$	$700^b (699^c)$	$603^b (604^c)$
$v_{ m HOCl}$	OH Bend	1396 (1398)	(1368)	1341 (1346)
$v_{ m OH_b}$	Bound OH Stretch	2385 (2384)	2603 (2602)	2903 (2903)

^a Value estimated as the difference between its experimentally observed combination with v_{OH_b} and the v_{OH_b} fundamental itself. ^b Value estimated as half the experimentally observed $v = 0 \rightarrow 2$ overtone transition.

365

366

367

368

369

370

371

372

373374

375

376

377

378

379380

381

382 383

384 385

386

Finally, we address the more complex interactions in play near the $v_{\rm OH_h}$ fundamental of the Br-HOCl complex (Figure 5b). To estimate the order of magnitude of the couplings, we first carried out a simple 2 \times 2 deperturbation scheme by considering the zero-order bright $v_{\rm OHb}$ transition interacting with an effective dark partner that manifests as the centroid of oscillator strength in the observed multiplet structure near 2800 cm⁻¹. This procedure yields an effective H_{Fermi} matrix element of 88 cm⁻¹, which is indeed intermediate between those found for the other two systems (66 and 99 cm⁻¹ for Cl and I, respectively) and included in **Table III**. Quantitative analysis of these interactions, however, requires treatment of the many levels involved as evidenced by the many transitions activated in this region. The occurrence of such multiplet structures in Fermi resonances are common,^{2,57} and result when several levels are in close proximity. One contribution to these arises in the Br-HOCl case because the bend fundamental is also engaged in a Fermi resonance interaction with the proximal $2v_{\text{oop}_H}$ level. Consequently, three levels $(4v_{\text{ooph}}, 2v_{\text{HOCl}}, \text{ and } v_{\text{HOCl}} + 2v_{\text{ooph}})$ now appear close to the $v_{\rm OH_h}$ fundamental in a classic example of a Fermi "polyad". See We therefore used our VPT2 code to explore the couplings among the nearly degenerate levels in Br $\bar{}$ +HOCl in the region of $v_{\mathrm{OH}_{\mathrm{h}}}$. The details of this analysis are presented in Section S3 of the Supplementary Material. To allow for comparison with the measured spectrum, the $v_{\rm HOCl} + 2v_{\rm oop_H}$ and $4v_{\rm oop_H}$ energy levels were estimated using the $2v_{\text{ooph}}$ value obtained in the analysis of the bend. This procedure recovers three transitions in the calculated Br-HOCl spectrum with significant intensity, which are assigned to the $4v_{\text{oop}_{\text{H}}}$, $2v_{\text{HOCl}}$, and $v_{\rm HOCl} + 2v_{\rm oop_H}$ transitions, and which fall close to the three closely spaced transitions in the observed spectrum. While the splittings among these peaks are roughly three times as large as those in the reported spectrum, this fine structure is expected to be very sensitive to both the magnitude of the Fermi coupling constant and the zero-order energies of the states. The existence of three transitions where only one is expected further supports the impact of the near degeneracy between $v_{\rm HOCl}$ and $2v_{\rm oop_H}$ in the lower

^c Theoretical value estimated as half the shifted $v = 0 \rightarrow 2$ overtone transition reported in **Table II**.

frequency region of the spectrum. Finally, this analysis also recovers a fourth transition with appreciable IR intensity that is assigned to $v_{\rm OH_b} + v_{\rm OX}$, which is in good agreement with the feature observed at 2841 cm⁻¹.

As was found to be the case in the $I^-\cdot H_2O$ system, part of the pervasive multiplet character of the bands near the v_{OH_b} fundamental arise from combination bands built on the bend overtone that fall near the v = 0 level of the OH stretch, and also undergo a Fermi resonance interaction with the v_{OH_b} v = 1 level, but with a much smaller matrix element. As with the Cl and I complexes, the $Br^-\cdot HOCl$ spectrum displays weaker bands displaced above the main features that are assigned to the in-plane rotation and ion-molecule translations and are included in **Table IV**. Note that the trends in these soft modes—decreasing from Cl to Br to I with values of 105 and 311, 83 and 235 (calculated), and 71 and 197 cm⁻¹, respectively—are in keeping with the qualitative picture of the H-bond becoming stronger and more directional for the smaller halides.

IV. SUMMARY

Anharmonic analysis of the vibrational band patterns displayed by the cryogenically cooled, H_2 -tagged $X^-\text{HOCl}$, (X = Cl, Br and I) complexes indicates that both electronic and mechanical anharmonicities contribute on a similar scale to the intensities of "extra bands" that occur across the vibrational spectrum. These nominally forbidden IR transitions gain oscillator strength due to intrinsic properties of the strong anionic H-bond. Specifically, the directionality of this interaction is associated with unusually large charge transfer (CT) along the acidic OH displacement toward the halide ion, which enhances the intensities and red shifts of the acidic OH stretch fundamentals for the smaller and more basic halide ions. Soft mode displacements that act to break this H-bond generate surprisingly strong overtones because these motions modulate the CT contribution. On the other hand, the strength of the anharmonic coupling (Fermi resonance) between the v = 1 level of the OH stretch and the v = 2 level of the intramolecular HOCl bend is similar to that found in the more weakly interacting $X^-\text{H}_2\text{O}$ systems, as evidenced by the characteristic matrix elements required to recover observed behavior in a simple (reduced dimensionality) interaction model.

SUPPLEMENTARY MATERIAL

See the Supplementary Material for detailed descriptions of the experimental setup, HOCl sample preparation, and additional computational details.

ACKNOWLEDGEMENTS

- This work was supported by NSF through the NSF Center for Aerosol Impacts on Chemistry of the
- 420 Environment (CAICE), CHE-1801971. Any opinions, findings, and conclusions or recommendations
- expressed in this material are those of the author(s) and do not necessarily reflect the views of the
- 422 National Science Foundation (NSF). Additionally, this work used the Extreme Science and Engineering
- Discovery Environment (XSEDE),⁵⁹ which is supported by grant number TG-CHE170064. A.B.M.
- acknowledges support from the Chemistry Division of the National Science Foundation (CHE-1856125

- for scientific work and OAC-1663636 for perturbation theory code development). Parts of this work were
- 426 performed using the Ilahie cluster at the University of Washington, which was purchased using funds
- from a MRI grant from the National Science Foundation (CHE-1624430). This work was also facilitated
- 428 through the use of advanced computational, storage, and networking infrastructure provided by the Hyak
- supercomputer system and funded by the STF at the University of Washington.

431

AUTHOR DECLARATIONS

432 Conflict of Interest

The authors have no conflicts to disclose.

434

435

433

DATA AVAILABILITY

The data that support the findings of this study are publicly available in a dataset hosted by the UCSD Library Digital Collections at: https://doi.org/10.6075/J0ZS2WPJ.

438

439

REFERENCES

- 440 [1] S. Horvath, A. B. McCoy, B. M. Elliott, G. H. Weddle, J. R. Roscioli, and M. A.
- Johnson, "Anharmonicities and Isotopic Effects in the Vibrational Spectra of X-H₂O, ·HDO, and ·D₂O [X =
- 442 Cl, Br, and I] Binary Complexes" J. Phys. Chem. A **114**, 1556-1568 (2010).
- 443 [2] J. J. Talbot, N. Yang, M. Huang, C. H. Duong, A. B. McCoy, R. P. Steele, and M. A.
- Johnson, "Spectroscopic Signatures of Mode-Dependent Tunnel Splitting in the Iodide-Water Binary
- 445 Complex" J. Phys. Chem. A **124**, 2991-3001 (2020).
- 446 [3] W. H. Robertson, and M. A. Johnson, "Molecular Aspects of Halide Ion Hydration: The Cluster
- 447 Approach" Annu. Rev. Phys. Chem. **54**, 173-213 (2003).
- 448 [4] J. R. Roscioli, E. G. Diken, M. A. Johnson, S. Horvath, and A. B. McCoy, "Prying apart a water
- 449 molecule with anionic H-bonding: a comparative spectroscopic study of the $X^- \cdot H_2O$ (X = OH, O, F, Cl, and
- 450 Br) binary complexes in the 600-3800 cm⁻¹ region" J. Phys. Chem. A **110**, 4943-4952 (2006).
- 451 [5] S. S. Xantheas, "Quantitative description of hydrogen bonding in chloride-water clusters" J. Phys.
- 452 Chem. 100, 9703-9713 (1996).
- 453 [6] A. B. McCoy, T. L. Guasco, C. M. Leavitt, S. G. Olesen, and M. A. Johnson, "Vibrational
- 454 Manifestations of Strong Non-Condon Effects in the H₃O⁺·X₃ (X = Ar, N₂, CH₄, H₂O) Complexes: A Possible
- Explanation for the Intensity in the "Association Band" in the Vibrational Spectrum of Water" Phys.
- 456 Chem. Chem. Phys. **14**, 7205-7214 (2012).
- 457 [7] S. Y. Liu, C. E. Dykstra, and D. J. Malik, "Electrical Effects on the Vibrational Transitions of
- 458 Hydrogen-Fluoride Due to Hydrogen-Bonding and Applied Fields" Chemical Physics Letters **130**, 403-409
- 459 (1986).
- 460 [8] D. W. Michael, C. E. Dykstra, and J. M. Lisy, "Changes in the Electronic-Structure and Vibrational
- 461 Potential of Hydrogen-Fluoride Upon Dimerization a Well-Correlated (HF)2 Potential-Energy Surface"
- 462 Journal of Chemical Physics **81**, 5998-6006 (1984).
- 463 [9] J. C. Morris, "Acid Ionization Constant of Hocl from 5 to 35 Degrees" J Phys Chem-Us 70, 3798-
- 464 3805 (1966).

- 465 [10] W. L. Marshall, and E. U. Franck, "Ion Product of Water Substance, 0°C-1000°C, 1-10,000 Bars -
- 466 New International Formulation and Its Background" J Phys Chem Ref Data 10, 295-304 (1981).
- 467 [11] W. R. Simpson, S. S. Brown, A. Saiz-Lopez, J. A. Thornton, and R. von Glasow, "Tropospheric
- 468 Halogen Chemistry: Sources, Cycling, and Impacts" Chem. Rev. 115, 4035-4062 (2015).
- 469 [12] M. J. Lawler, R. Sander, L. J. Carpenter, J. D. Lee, R. von Glasow, R. Sommariva, and E. S.
- 470 Saltzman,"HOCl and Cl₂ observations in marine air" Atmos Chem Phys **11**, 7617-7628 (2011).
- 471 [13] S. Pechtl, and R. von Glasow, "Reactive chlorine in the marine boundary layer in the outflow of
- 472 polluted continental air: A model study" Geophys Res Lett **34**, (2007).
- 473 [14] R. Vogt, P. J. Crutzen, and R. Sander, "A mechanism for halogen release from sea-salt aerosol in
- 474 the remote marine boundary layer" Nature **383**, 327-330 (1996).
- 475 [15] A. K. Huff, and J. P. D. Abbatt, "Kinetics and product yields in the heterogeneous reactions of
- HOBr with ice surfaces containing NaBr and NaCl" Journal of Physical Chemistry A **106**, 5279-5287
- 477 (2002).
- 478 [16] J. P. D. Abbatt et al.,"Halogen activation via interactions with environmental ice and snow in the
- polar lower troposphere and other regions" Atmos Chem Phys 12, 6237-6271 (2012).
- 480 [17] C. B. Faxon, and D. T. Allen, "Chlorine Chemistry in Urban Atmospheres: A Review" Environ Chem
- 481 **10**, 221-233 (2013).
- 482 [18] N. Yang, C. H. Duong, P. J. Kelleher, M. A. Johnson, and A. B. McCoy, "Isolation of Site-Specific
- 483 Anharmonicities of Individual Water Molecules in the I⁻⋅(H₂O)₂ Complex Using Tag-Free, Isotopomer
- 484 Selective IR-IR Double Resonance" Chem. Phys. Lett. **690**, 159-171 (2017).
- 485 [19] F. S. Menges, E. H. Perez, S. C. Edington, C. H. Duong, N. Yang, and M. A. Johnson, "Integration of
- 486 High-Resolution Mass Spectrometry with Cryogenic Ion Vibrational Spectroscopy" J. Am. Soc. Mass
- 487 Spectrom. **30**, 1551-1557 (2019).
- 488 [20] A. B. Wolk, C. M. Leavitt, E. Garand, and M. A. Johnson, "Cryogenic Ion Chemistry and
- 489 Spectroscopy" Accounts Chem Res **47**, 202-210 (2014).
- 490 [21] M. A. Boyer, and A. B. McCoy,"A Flexible Approach to Vibrational Perturbation Theory Using
- 491 Sparse Matrix Methods" J Chem Phys **156**, 054107, JCP21-AR-04320. (2022).
- 492 [22] M. A. Boyer, and A. B. McCoy, PyVibPTn, a General Package for Vibrational Perturbation Theory,
- 493 (2021), 10.5281/zenodo.5563091.
- 494 [23] J. J. Sakurai, Modern Quantum Mechanics (Addison-Wesley Publishing Company, Inc., 1994),
- 495 Revised edn.
- 496 [24] M. J. Frisch et al., Gaussian 16 Rev. B.01, (2016).
- 497 [25] E. D. Glendening, A. E. Reed, J. E. Carpenter, and F. Weinhold, NBO Version 3.1.
- 498 [26] K. A. Peterson, D. Figgen, E. Goll, H. Stoll, and M. Dolg, "Systematically Convergent Basis Sets
- 499 with Relativistic Pseudopotentials. II. Small-Core Pseudopotentials and Correlation Consistent Basis Sets
- 500 for the Post-d Group 16-18 Elements" J. Chem. Phys. **119**, 11113-11123 (2003).
- 501 [27] K. A. Peterson, B. C. Shepler, D. Figgen, and H. Stoll, "On the Spectroscopic and Thermochemical
- 502 Properties of ClO, BrO, IO, and Their Anions" J. Phys. Chem. A 110, 13877-13883 (2006).
- 503 [28] M. Z. Kamrath, E. Garand, P. A. Jordan, C. M. Leavitt, A. B. Wolk, M. J. Van Stipdonk, S. J. Miller,
- and M. A. Johnson, "Vibrational Characterization of Simple Peptides Using Cryogenic Infrared
- Photodissociation of H₂-tagged, Mass-selected Ions" Journal of the Amercian Chemical Society **133**,
- 506 6440-6448 (2011).
- 507 [29] G. Cavallo, P. Metrangolo, R. Milani, T. Pilati, A. Priimagi, G. Resnati, and G. Terraneo, "The
- 508 Halogen Bond" Chem. Rev. **116**, 2478-2601 (2016).
- 509 [30] J. S. Francisco,"An ab initio study of the structure and stability of Cl⁻ HOCl anionic complex"
- 510 Chemical Physics Letters **260**, 485-491 (1996).

- 511 [31] B. A. Flowers, and J. S. Francisco, "Ab Initio Characterization of the Structure, Vibrational, and
- 512 Energetic Properties of Br · HOCl, Cl · HOBr, and Br · HOBr Anionic Complexes" J. Phys. Chem. A 105,
- 513 494-500 (2001).
- 514 [32] X. X. Zhang, G. X. Liu, S. Ciborowski, W. Wang, C. Gong, Y. F. Yao, and K. Bowen, "Spectroscopic
- 515 Measurement of a Halogen Bond Energy" Angew. Chem. Int. Ed. 58, 11400-11403 (2019).
- 516 [33] R. A. Ashby, "Infrared Spectrum of HOCI" J. Mol. Spectrosc. **23**, 439-447 (1967).
- 517 [34] N. Yang, C. H. Duong, P. J. Kelleher, and M. A. Johnson, "Capturing Intrinsic Site-Dependent
- 518 Spectral Signatures and Lifetimes of Isolated OH Oscillators in Extended Water Networks" Nat. Chem.
- **12**, 159-164 (2020).
- 520 [35] T. Shimanouchi, Tables of Molecular Vibrational Frequencies Consolidated Volume I, National
- 521 Bureau of Standards 1972).
- 522 [36] R. A. Ashby, "Infrared Spectrum of HOCI" J. Mol. Spectrosc. **40**, 639-640 (1971).
- 523 [37] A. B. McCoy, X. Huang, S. Carter, and J. M. Bowman, "Quantum Studies of H3O2- and D3O2-" J.
- 524 Chem. Phys. **123**, 064317 (2005).
- 525 [38] E. G. Diken, J. M. Headrick, J. R. Roscioli, J. C. Bopp, M. A. Johnson, and A. B.
- McCoy, "Fundamental Excitations of the Shared Proton in the $H_3O_2^-$ and $H_5O_2^+$ Complexes" J. Phys.
- 527 Chem. A **109**, 1487-1490 (2005).
- 528 [39] G. C. Pimentel, "The Bonding of Trihalide and Bifluoride Ions by the Molecular Orbital Method"
- 529 Journal of Chemical Physics **19**, 446-448 (1951).
- 530 [40] Q. Yu, and J. M. Bowman,"How the Zundel ($H_5O_2^+$) Potential Can Be Used to Predict the Proton
- 531 Stretch and Bend Frequencies of Larger Protonated Water Clusters" Journal of Physical Chemistry
- 532 Letters **7**, 5259-5265 (2016).
- 533 [41] N. Yang, T. Khuu, S. Mitra, C. H. Duong, M. A. Johnson, R. J. DiRisio, A. B. McCoy, E. Miliordos,
- and S. S. Xantheas, "Isolating the Contributions of Specific Network Sites to the Diffuse Vibrational
- 535 Spectrum of Interfacial Water with Isotopomer-Selective Spectroscopy of Cold Clusters" J. Phys. Chem. A
- 536 **124**, 10393-10406 (2020).
- 537 [42] J. E. Bartmess, in NIST Chemistry WebBook, NIST Standard Reference Database Number 69,
- edited by P. J. Linstrom, and W. G. Mallard (National Institute of Standards and Technology,
- 539 Gaithersburg MD.
- 540 [43] T. K. Ghanty, and S. K. Ghosh, "Proton affinity and acidity of hypohalous acids: A density
- 541 functional study" Journal of Physical Chemistry A 101, 5022-5025 (1997).
- 542 [44] J. P. Foster, and F. Weinhold, "Natural Hybrid Orbitals" J. Am. Chem. Soc. **102**, 7211-7218 (1980).
- 543 [45] A. E. Reed, and F. Weinhold, "Natural Bond Orbital Analysis of near-Hartree-Fock Water Dimer" J.
- 544 Chem. Phys. **78**, 4066-4073 (1983).
- 545 [46] A. E. Reed, R. B. Weinstock, and F. Weinhold, "Natural-Population Analysis" J. Chem. Phys. 83,
- 546 735-746 (1985).
- 547 [47] A. E. Reed, and F. Weinhold, "Natural Localized Molecular-Orbitals" J. Chem. Phys. 83, 1736-1740
- 548 (1985).
- 549 [48] J. E. Carpenter, (University of Wisconsin, Madison, 1987).
- J. E. Carpenter, and F. Weinhold, "Analysis of the Geometry of the Hydroxymethyl Radical by the
- Different Hybrids for Different Spins Natural Bond Orbital Procedure" J. Mol. Struc. Theochem 169, 41-
- 552 62 (1988).
- 553 [50] A. E. Reed, L. A. Curtiss, and F. Weinhold,"Intermolecular Interactions from a Natural Bond
- Orbital, Donor-Acceptor Viewpoint" Chem. Rev. 88, 899-926 (1988).
- 555 [51] F. Weinhold, and J. E. Carpenter, The Structure of Small Molecules and Ions (Plenum, New York,
- 556 1988).

- 557 [52] J. J. Talbot, N. Yang, M. Huang, C. H. Duong, A. B. McCoy, R. P. Steele, and M. A.
- 558 Johnson, "Spectroscopic Signatures of Mode-Dependent Tunnel Splitting in the Iodide-Water Binary
- 559 Complex" Journal of Physical Chemistry A **124**, 2991-3001 (2020).
- 560 [53] W. H. Robertson, G. H. Weddle, J. A. Kelley, and M. A. Johnson, "Solvation of the Cl⁻⋅H₂O
- 561 Complex in CCl₄ Clusters: The Effect of Solvent-Mediated Charge Redistribution on the Ionic H-Bond" J.
- 562 Phys. Chem. A **106**, 1205-1209 (2002).
- 563 [54] J. C. Werhahn, D. Akase, and S. S. Xantheas, "Universal scaling of potential energy functions
- describing intermolecular interactions. II. The halide-water and alkali metal-water interactions" Journal
- of Chemical Physics **141**, (2014).
- 566 [55] N. Yang, C. H. Duong, P. J. Kelleher, A. B. McCoy, and M. A. Johnson, "Deconstructing Water's
- Diffuse OH Stretching Vibrational Spectrum With Cold Clusters" Science **364**, 275-278 (2019).
- 568 [56] P. Ayotte, G. H. Weddle, J. Kim, and M. A. Johnson, "Vibrational Spectroscopy of the Ionic
- Hydrogen Bond: Fermi Resonances and Ion-Molecule Stretching Frequencies in the Binary $X^-(H_2O)$ (X =
- 570 Cl, Br, I) Complexes via Argon Predissociation Spectroscopy" J. Am. Chem. Soc. 120, 12361-12362 (1998).
- 571 [57] A. F. DeBlase, S. Bloom, T. Lectka, K. D. Jordan, A. B. McCoy, and M. A. Johnson, "Origin of the
- 572 Diffuse Vibrational Signature of a Cyclic Intramolecular Proton Bond: Anharmonic Analysis of Protonated
- 573 1,8-disubstituted Naphthalene Ion" J. Chem. Phys. **139**, 024301 (2013).
- 574 [58] M. R. Berman, Emerging trends in chemical applications of lasers (American Chemical Society,
- 575 Washington, 2021), ACS symposium series, 1398.
- 576 [59] J. Towns, T. Cockerill, M. Dahan, I. Foster, K. Gaither, A. Grimshaw, C. Hazlewood, S. Lathrop, D.
- 577 Lifka, G. D. Peterson, R. Roskies, J. R. Scott, and N. Wilkins-Diehr, "XSEDE: Accelerating Scientific
- 578 Discovery" Comput. Sci. Eng. **16**, 62-74 (2014).